

Ground-state phase diagram of the one-dimensional Hubbard-model with an alternating potential

Hiromi Otsuka¹ and Masaaki Nakamura²

¹*Department of Physics, Tokyo Metropolitan University, Tokyo 192-0397 Japan*

²*Department of Applied Physics, Faculty of Science,
Tokyo University of Science, Tokyo 162-8601 Japan*

(Dated: May 23, 2019)

We investigate the ground-state phase diagram of the one-dimensional half-filled Hubbard model with an alternating potential — a model for the charge-transfer organic materials and the ferroelectric perovskites. We numerically determine the global phase diagram of this model using the level-crossing and the phenomenological renormalization-group methods based on the exact diagonalization calculations. Our results support the mechanism of the double phase transitions between Mott and a band insulators pointed out by Fabrizio, Gogolin, and Nersesyan: We confirm the existence of the spontaneously dimerized phase as an intermediate state. Further we provide numerical evidences to check the criticalities on the phase boundaries. Especially, we perform the finite-size-scaling analysis of the excitation gap to show the two-dimensional Ising transition in the charge part. On the other hand, we confirm that the dimerized phase survives in the strong-coupling limit, which is one of the resultants of competition between the ionicity and correlation effects.

PACS numbers: 71.10.Pm, 71.30.+h

I. INTRODUCTION

The electronic and/or magnetic properties of the low-dimensional interacting electrons have attracted great interest in researches of novel materials such as the quasi one-dimensional (1D) organic compounds and the two-dimensional (2D) high- T_c cuprates, where a variety of generalized Hubbard-type models have been introduced.¹ For the 1D case, a concept of the Tomonaga-Luttinger liquid (TLL) has been widely accepted, and intensively used not only for the descriptions on the low-energy and long-distance behaviors of the critical systems,^{2,3,4} but also for the prediction of its instabilities to, for instance, various types of density-wave phases observed in the models.⁵

The 1D Hubbard model with an alternating potential (also called the ionic Hubbard model) is one of the models for the π -electron charge-transfer organic materials such as TTF-Chloranil⁶ and/or the ferroelectric transition metal oxides as BaTiO₃.^{7,8} It is defined by the Hamiltonian

$$H = -t \sum_{j,s} \left(c_{j,s}^\dagger c_{j+1,s} + \text{H.c.} \right) + \sum_j U n_{j,\uparrow} n_{j,\downarrow} + \sum_j \Delta (-1)^j n_j, \quad (1)$$

where $c_{j,s}$ annihilates an s -spin electron ($s = \uparrow$ or \downarrow) on the j th site and the number operator $n_{j,s} = c_{j,s}^\dagger c_{j,s}$ and $n_j = n_{j,\uparrow} + n_{j,\downarrow}$. While t and U terms stand for the electron transfer among sites and the Coulomb repulsion on the same site, respectively, the Δ term represents an energy difference between the donor and acceptor molecules (or between the cation and oxygen atoms), and it introduces ionicity effects into the correlated electron systems (we set $t = 1$ in the following discussion).

The understandings on the model have been accumulated in the literature, where the theoretical investigations including numerical calculations have been performed mainly at the half-filling: Nagaosa and Takimoto calculated the magnetic and charge-transfer gaps as functions of Δ (U fixed) by using the quantum Monte Carlo (QMC) simulation.⁶ Resta and Sorella, using the exact-diagonalization calculations of finite size systems, reported, for instance, the divergence of the average dynamical charge.⁹ By applying the renormalization-group (RG) method to the bosonized Hamiltonian, Tsuchiizu and Suzumura estimated a boundary line between the Mott insulator (MI) and a band insulator (BI) phases in the weak-coupling regions.⁸ On the other hand, Fabrizio, Gogolin, and Nersesyan (FGN) predicted an existence of the “spontaneously dimerized insulator (SDI)” phase between them.^{10,11}

After their proposal, various numerical calculation methods have been so far applied to confirm it: Wilkens and Martin performed the QMC simulations to evaluate, e.g., the bond order parameter, and reported the transition between the BI and SDI phases and stated an absence of MI phase for $\Delta > 0$.¹² By the combined use of the method of topological transitions (jumps in charge and spin Berry phases)^{9,13,14,15} and the method of crossing excitation levels, Torio *et al.* provided a global ground-state phase diagram, which is in accord with the FGN scenario.¹⁶ And an existence of the SDI phase for all $U > 0$ regions was first exhibited there. The density matrix renormalization group (DMRG) calculations^{17,18,19,20} have been performed by several groups. For instance, Zhang *et al.* provided the data on the structure factors of relevant order parameters in the weak- and intermediate-coupling region, which supports an existence of intermediate SDI phase between the BI and MI phases.¹⁹ On one hand, Kampf *et al.* es-

timated the excitation gaps up to 512 site system and found the boundary of the BI phase while the existence of the second boundary was not resolved.²⁰ Therefore, some controversy as well as points of agreement exists in these recent investigations.

In this paper using the standard numerical techniques, we shall provide both the global structure of the ground-state phase diagram and the evidences to show the criticalities of the massless spin and charge parts. For this purpose, it is worthy of noticing that the FGN scenario consists of two types of instabilities commonly observed in the TLL, i.e., the transition with the SU(2)-symmetric Gaussian criticality in the spin part, and that with the 2D-Ising criticality in the charge part (see Sec. II). Further, these types of phase transitions have been numerically treated by the level-crossing (LC) method, and the phenomenological renormalization-group (PRG) method.²¹ The LC method was first applied to the frustrated XXZ chain.^{22,23} This method has been also used in the researches of higher- S spin chains,²⁴ spin ladders,²⁵ and 1D correlated electron systems.^{26,27} The advantage of using the LC method is not restricted to its accuracy in estimating the continuous phase transition points including the Berezinskii-Kosterlitz-Thouless type one; it also provides a means to check their criticalities (see Sec. III).²³ Both of these are important in order to settle the controversy mentioned above, and in fact the precise estimation of the spin-gap transition point of the $S = \frac{1}{2}$ J_1 - J_2 chain was first given by the LC method,²² while numerical investigations including the DMRG work were performed. On the other hand, the PRG method is also a reliable numerical approach to determine second-order phase transition point, especially for the 2D-Ising transition where the LC method is not available. Analysis based on the PRG method for the 2D-Ising transition is successful in the spin systems.²⁴ Further, one of the authors treated the 2D-Ising transition in the $S = \frac{1}{2}$ J_1 - J_2 model under a staggered magnetic field, where the critical phenomena in the vicinity of the phase boundary line were argued.²⁸ Therefore, based on these recent developments, we shall perform the numerical calculations; especially, to our knowledge, this is the first time that the PRG method successfully applied to the 2D-Ising transition observed in one part of the two-component systems like the interacting electrons.

The organization of this paper is as follows. In Sec. II, we shall briefly refer to the effective theory based on the bosonized Hamiltonian and order parameters of expected density-wave phases, and mention the FGN scenario. In Sec. III, we explain procedures of the numerical calculation to determine transition lines, where connections between the methods and instabilities of the TLL systems will be explained. After that, we shall give a ground-state phase diagram in whole parameter region. Further, to confirm the criticalities and to serve a reliability of our calculations, we check the consistency of excitation levels in finite-size systems. A finite-size-scaling analysis of the charge excitation gaps is also performed in the vicinity of

the phase boundary line. Section IV is devoted to discussions and summary of the present investigation. A short comment on the Berry phase method^{9,13,14,15,16} will be also given there. We will provide the comparison with that method, which is helpful to exhibit a reliability of our approach as well as the results.

II. GROUND STATES AND PHASE TRANSITIONS

The bosonization method provides an efficient way to describe low-energy properties of the 1D quantum systems:²⁹ Linearizing the cos-band at two Fermi points $\pm k_F = \pm \pi n/2a$ [an electron density $n := N/L = 1$ and a number of sites (electrons) L (N)], and according to standard procedure, the effective Hamiltonian^{8,10,11} is given as $H \rightarrow \mathcal{H} = \mathcal{H}_\rho + \mathcal{H}_\sigma + \mathcal{H}_2$ with

$$\mathcal{H}_\nu = \int dx \frac{v_\nu}{2\pi} \left[K_\nu (\partial_x \theta_\nu)^2 + \frac{1}{K_\nu} (\partial_x \phi_\nu)^2 \right] + \int dx \frac{2g_\nu}{(2\pi\alpha)^2} \cos \sqrt{8}\phi_\nu, \quad (\nu = \rho, \sigma), \quad (2)$$

$$\mathcal{H}_2 = \int dx \frac{-2\Delta}{\pi\alpha} \sin \sqrt{2}\phi_\rho \cos \sqrt{2}\phi_\sigma. \quad (3)$$

The operator θ_ν is the dual field of ϕ_ν satisfying the commutation relation $[\phi_\nu(x), \partial_y \theta_{\nu'}(y)/\pi] = i\delta(x-y)\delta_{\nu,\nu'}$. K_ν and v_ν are the Gaussian coupling and the velocity of elementary excitations. Coupling constants g_ρ (< 0) and g_σ stand for the $4k_F$ -Umklapp scattering and the backward scattering bare amplitudes, respectively, and \mathcal{H}_2 expresses a coupling between the spin and charge degrees of freedom. In TABLE I, we summarize the order parameters for the relevant $2k_F$ density-wave phases, i.e., the charge-density-wave (CDW), bond charge-density-wave (BCDW), and spin-density-wave (SDW) phases, where the electron's spin and the bond charge are given as $\mathbf{S}_j = \sum_{s,s'} c_{j,s}^\dagger [\frac{1}{2}\boldsymbol{\sigma}]_{s,s'} c_{j,s'}$ and $\bar{n}_j = \sum_s (c_{j,s}^\dagger c_{j+1,s} + \text{H.c.})$, respectively ($\boldsymbol{\sigma}$ are the Pauli matrices). Their bosonized expressions are given in the second column. In the third column, we give the locking points of phase fields. As discussed in Ref. 10, there are two locking points of ϕ_ρ , i.e., $\langle \sqrt{8}\phi_\rho \rangle = \pm\phi_0$ in the SDW and BCDW states. The phase ϕ_0 , a function of U and Δ , continuously varies from 0 ($\Delta = 0$) to π .

Let us see the system with increasing Δ for fixed U . At $\Delta = 0$, the ground state is in the MI phase with the most divergent SDW fluctuation (the third row of TABLE I). According to the arguments,^{6,8} the MI phase may survive for $U \gg 2\Delta$. On the other hand, for $2\Delta \gg U$, \mathcal{H}_2 becomes relevant, and leads to the BI phase with the long-range CDW order without degeneracy (the first row of TABLE I). For this issue, FGN argued that under the uniform charge distribution a renormalization effect of \mathcal{H}_2 to g_σ brings about the spin-gap transition in the spin part at a certain value of $\Delta_\sigma(U)$ which is described by the sine-Gordon (SG) theory. This is qualitatively in

TABLE I: The order parameters. The bosonized forms and the locking points of phase variables ($\langle\sqrt{8}\phi_\rho\rangle, \langle\sqrt{8}\phi_\sigma\rangle$) are given in the second and third columns. ϕ_0 is a function of U and Δ , and “*” denotes a phase not to be locked.

Order parameters	Bosonized forms	Locking points
$\mathcal{O}_{\text{CDW}} = (-1)^j n_j$	$2 \sin \sqrt{2}\phi_\rho \cos \sqrt{2}\phi_\sigma$	$(\pi, 0)$
$\mathcal{O}_{\text{BCDW}} = (-1)^j \bar{n}_j$	$2 \cos \sqrt{2}\phi_\rho \cos \sqrt{2}\phi_\sigma$	$(\pm\phi_0, 0)$
$\mathcal{O}_{\text{SDW}}^\parallel = (-1)^j S_j^z$	$2 \cos \sqrt{2}\phi_\rho \sin \sqrt{2}\phi_\sigma$	$(\pm\phi_0, *)$

accord with the perturbation calculation in the strong-coupling region,⁶ and leads to the SDI phase with the long-range BCDW order (the second row). Further with the increase of Δ , a transition in the charge part occurs on a separatrix $\Delta_\rho(U)$ between two different types of charge-gap states. This line corresponds to the massless RG flow connecting the Gaussian (the central charge $c = 1$) and the 2D-Ising ($c = \frac{1}{2}$) fixed points,³⁰ and its description is given by the double-frequency sine-Gordon (DSG) theory.³¹ Our main task is thus to estimate $\Delta_\nu(U)$ for $U > 0$ and to check the criticalities based on their prediction.

III. NUMERICAL METHODS AND CALCULATION RESULTS

Low-lying excitations observed in the finite-size systems are expected to serve for the determinations of transition points. Here, we take a look at the following operators with lower scaling dimensions:

$$\mathcal{O}_{\nu,1} = \sqrt{2} \cos \sqrt{2}\phi_\nu, \quad (4)$$

$$\mathcal{O}_{\nu,2} = \sqrt{2} \sin \sqrt{2}\phi_\nu, \quad (5)$$

$$\mathcal{O}_{\nu,3} = \exp(\pm i\sqrt{2}\theta_\nu). \quad (6)$$

According to the finite-size-scaling argument based on the conformal field theory, corresponding energy levels for these operators $\Delta E_{\nu,i}$ (taking the ground-state energy E_0 as zero) are expressed by the use of their scaling dimensions $x_{\nu,i}$.³²

$$\Delta E_{\nu,i} \simeq \frac{2\pi v_\nu}{L} x_{\nu,i}. \quad (7)$$

Then these excitations can be extracted under anti-periodic boundary conditions with respect to the ground state due to the selection rule of the quantum numbers.^{26,27} Here note that in the numerical calculations using the Lanczos algorithm we can identify $\Delta E_{\nu,i}$ according to the discrete symmetries of the wave functions, e.g., translation ($c_{j,s} \rightarrow c_{j+2,s}$), charge conjugation ($c_{j,s} \rightarrow (-1)^j c_{j+1,s}^\dagger$), spin reverse ($c_{j,s} \rightarrow c_{j,-s}$), and space inversion ($c_{j,s} \rightarrow c_{L-j,s}$). Except for the spin reversal operation, definitions of these transformations are different from those of the uniform systems such as the extended Hubbard model.²⁷

First, we treat the spin-gap transition in the spin part following Refs. 22,26,27. In the SDW phase, due to the marginal coupling in the SU(2)-symmetric spin part, the singlet ($x_{\sigma,1}$) and triplet ($x_{\sigma,2} = x_{\sigma,3}$) excitations split as $x_{\sigma,1} > x_{\sigma,2} = x_{\sigma,3}$ satisfying an universal relation

$$\frac{x_{\sigma,1} + 3x_{\sigma,2}}{4} = \frac{1}{2}. \quad (8)$$

Then, the degeneracy condition

$$x_{\sigma,1} = x_{\sigma,2} = x_{\sigma,3} \quad (9)$$

stands for the vanishing of the coupling, and provides a good estimation of the spin-gap transition point. Note that Torio *et al.* used the crossing of these excitation levels for the determination of the MI-SDI transition,¹⁶ while the consistency check of the levels to confirm the universality of transition is still absent. Figure 1 shows an example of the Δ dependences of $x_{\sigma,i}$ for the 16-site system at $u = 0.6$ [here we introduce the reduced Coulomb interaction parameter $u = U/(U + 4)$]. For this plot, we estimated the spin-wave velocity v_σ from a triplet excitation with the wave number $4\pi/L$ as $v_\sigma = \lim_{L \rightarrow \infty} \Delta E(S = 1, k = 4\pi/L)/(2\pi/L)$ and normalized the excitation gaps $\Delta E_{\sigma,i}$ according to Eq. (7). The singlet (triplet) level corresponding to the operator $\mathcal{O}_{\sigma,1}$ [$\mathcal{O}_{\sigma,2}$ ($\mathcal{O}_{\sigma,3}$)] is denoted by circles (triangles) with a fitting curve. Their behaviors reflect the TLL properties: For instance, the amplitude of the level splitting decreases with the increase of Δ due to its renormalization effect, and eventually the level crossing occurs at $\Delta_\sigma(U, L)$. More precisely, in order to confirm the universality, we plot the averaged scaling dimension x_{av} , i.e., the left hand side of Eq. (8) in the figure (squares). We also exhibit the L -dependence of x_{av} at $\Delta = 1.0$ as an example (see the inset). The result shows that the condition imposed on $x_{\sigma,i}$ is accurately satisfied for $\Delta \leq \Delta_\sigma(U, L)$; in particular, the extrapolated value of x_{av} is almost $\frac{1}{2}$. Consequently, the level crossing at which Eq. (9) is satisfied can be regarded as an indication of the spin-gap transition in the spin part of the Hamiltonian (1). On the other hand, the spin part is dimerized for $\Delta > \Delta_\sigma(U, L)$.

Next, we discuss the 2D-Ising transition in the charge part. Recently, we have treated the crossover behavior into the 2D-Ising criticality in the study of the frustrated quantum spin chain,²⁸ so we shall here employ the same approach to determine $\Delta_\rho(U)$. Since there are two critical fixed points connected by the RG flow, a relationship between lower-energy excitations on these fixed points is quite important. For this, the so-called ultraviolet-infrared (UV-IR) operator correspondence provides significant informations.^{11,33} Along the RG flow, the operators on the Gaussian fixed point (UV) are transmuted to those on the 2D-Ising fixed point (IR) as

$$\mathcal{O}_{\rho,1} \rightarrow \mu, \quad \mathcal{O}_{\rho,2} \rightarrow I + \epsilon, \quad (10)$$

where μ is the disorder field (Z_2 odd), and ϵ is the energy density operator (Z_2 even) with scaling dimensions

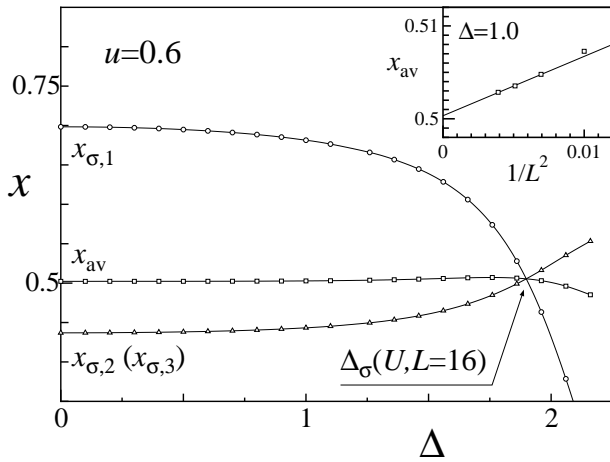


FIG. 1: The Δ dependence of $x_{\sigma,i}$ at $u = 0.6$ for the 16-site system [$u = U/(U + 4)$]. The spin-gap transition point $\Delta_\sigma(U, L)$ is estimated from the level crossing between the singlet (circles) and triplet (triangles) spin excitations. The squares plot $x_{\text{av}} = (x_{\sigma,1} + 3x_{\sigma,2})/4$, and the inset shows the L -dependence of x_{av} at $\Delta = 1.0$, where a least-square-fitting line to the data of $L = 12$ -16 is given.

$x_\mu = \frac{1}{8}$ and $x_\epsilon = 1$, respectively. Further, since a deviation from the transition point $\Delta - \Delta_\rho(U)$ which is the coupling constant of the $\mathcal{O}_{\rho,2}$ term in the DSG Hamiltonian¹⁰ plays a role of the thermal scaling variable, anomalous behaviors in the vicinity of $\Delta_\rho(U)$ are to be related to the divergent correlation length of the form $\xi \propto [\Delta - \Delta_\rho(U)]^{-\nu}$ with the exponent $1/\nu = 2 - x_\epsilon = 1$. On one hand, the excitation μ corresponding to $\mathcal{O}_{\rho,1}$ provides a lower-energy level, so we shall focus our attention on it. In order to determine the transition point, we shall numerically solve the following PRG equation for a given value of U with respect to Δ .^{21,28}

$$(L + 2)\Delta E_{\rho,1}(U, \Delta, L + 2) = L\Delta E_{\rho,1}(U, \Delta, L). \quad (11)$$

Since this is satisfied by the gap $\Delta E_{\rho,1}(U, \Delta, L) \propto 1/L$, the obtained value can be regarded as the L -dependent transition point, say $\Delta_\rho(U, L + 1)$. We plot L and Δ dependences of the scaled gap $L\Delta E_{\rho,1}(U, \Delta, L)$ in Fig. 2, and find that the size dependence of the crossing point is small for large values of U , but it is visible in the weak coupling case.

While the results in the thermodynamic limit will be given in the last part of this section, we shall check first the criticality on and in the vicinity of the phase boundary using the extrapolated data $\Delta_\rho(U)$. For this aim, an evaluation of the central charge c through the size dependence of the ground-state energy provides a straight forward way.³⁴ However, as exhibited in the following, the critical line in the charge part is close to the spin-gap transition line, so that influences from the spin part with the small dimer gap prohibit a reliable estimation of c from the data of the finite-size systems. Alternatively,

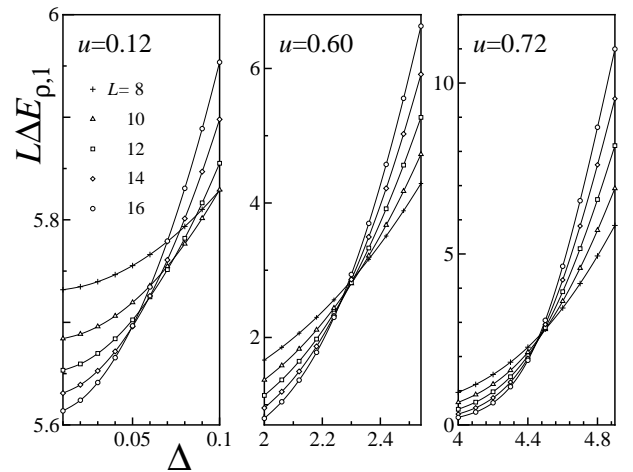


FIG. 2: The L and Δ dependences of the scaled gap $L\Delta E_{\rho,1}$. From left to right, $u = 0.12, 0.60$ and 0.72 , respectively. The correspondence between marks and system sizes is given in the figure. Crossing points give the L -dependent transition points $\Delta_\rho(U, L + 1)$.

we shall evaluate a ratio of the charge-excitation gaps $\Delta E_{\rho,1}(U, \Delta, L)$ and $\Delta E_{\rho,2}(U, \Delta, L)$ on the phase boundary to check the UV-IR operator correspondence. According to Eqs. (7) and (10), it is expressed by the scaling dimensions of operators ϵ and μ as

$$R = \frac{\Delta E_{\rho,1}(U, \Delta_\rho(U), L)}{\Delta E_{\rho,2}(U, \Delta_\rho(U), L)} \rightarrow \frac{x_\mu}{x_\epsilon} = \frac{1}{8} \quad (12)$$

for large L . Figure 3 plots the Δ dependence of R for $L = 10$ -16 ($u = 0.72$). The transition point in the thermodynamic limit is denoted by the arrow near the x -axis. While the ratio exhibits a subtle Δ dependence around the point, we interpolate these data, and estimate the L -dependence of R at $\Delta_\rho(U)$, which is given with a least-square-fitting line in the inset. The plot shows that the extrapolated value is fairly close to $\frac{1}{8}$. Therefore we conclude that the boundary line $\Delta_\rho(U)$ belongs to the 2D-Ising universality class.

Further, we shall investigate the critical behavior.²⁸ According to the finite-size-scaling argument, we analyze the charge-excitation gap by using the following one-parameter scaling form

$$\Delta E_{\rho,1}(U, \Delta, L) = L^{-1}\Psi(L[\Delta - \Delta_\rho(U)]^\nu). \quad (13)$$

Since $\Delta E_{\rho,1} \propto 1/\xi$ in the thermodynamic limit ($L/\xi \rightarrow \infty$), the scaling function is expected to asymptotically behave as $\Psi(x) \propto x$ for large x . On the other hand, the gap $\Delta E_{\rho,1} \propto 1/L$ on the critical point ($L/\xi \rightarrow 0$) so that $\Psi(x) \simeq \text{const.}$ for $x \rightarrow 0$.³⁵ Figure 4 plots Eq. (13) using the exponent of the 2D-Ising model $\nu = 1$. Although due to the smallness of L a scattering of the scaled data is visible especially near the transition point, the data of different system sizes are collapsed on the single curve, and

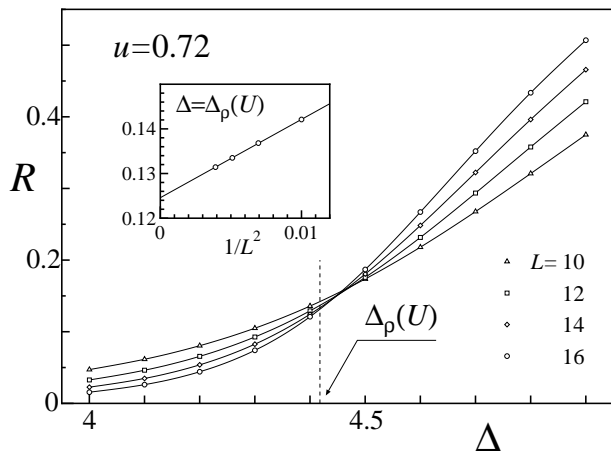


FIG. 3: The Δ dependence of the charge-excitation-gap ratio $R = \Delta E_{\rho,1}(U, \Delta, L) / \Delta E_{\rho,2}(U, \Delta, L)$ for $L = 10-16$ at $u = 0.72$. The arrow shows the transition point $\Delta_{\rho}(U)$. The inset plots the L -dependence of R at $\Delta_{\rho}(U)$ with a least-square-fitting line.

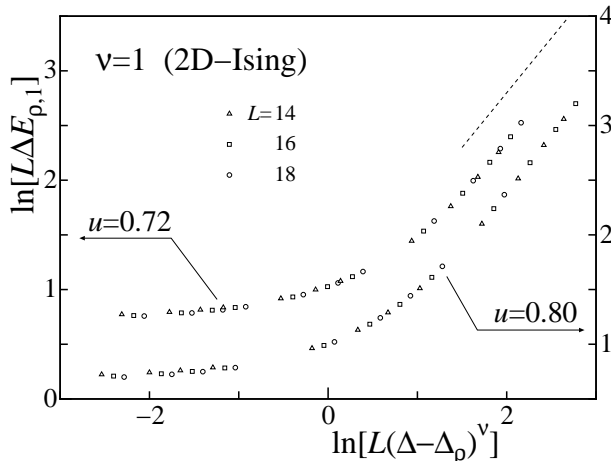


FIG. 4: The finite-size-scaling plots of the charge-excitation gap $\Delta E_{\rho,1}$ for systems of $L = 14-18$ at $u = 0.72$ and 0.80 . We use the 2D-Ising critical exponent $\nu = 1$. A dotted line (the slope 1) is given for the guide to eye.

its asymptotic behaviors agree with the expected ones. Therefore, we can check that, in the transition of the charge part, the deviation $\Delta - \Delta_{\rho}(U)$ plays a role of the thermal scaling variable on the 2D-Ising fixed point. Here, note that in the strong-coupling region the energy scale of the crossover behavior may be large enough to be detected even in the small-size systems. However, the finite-size-scaling nature may become obscure in the weak and intermediate couplings.

Lastly, we present the ground-state phase diagram. In order to determine it, the extrapolations of $\Delta_{\nu}(U, L)$ to the thermodynamic limit are carried out. For the spin

part, it should be noted that Torio *et al.* evaluated the spin-gap transition line from the level crossing Eq. (9),¹⁶ so here we perform the same calculations in order to complete the ground-state phase diagram. We employ the formula: $\Delta_{\sigma}(U, L) = \Delta_{\sigma}(U) + aL^{-2} + bL^{-4}$, where $\Delta_{\sigma}(U)$, a and b are determined according to the least-square-fitting condition. Then, we extrapolated the data of $L = 12-18$ as shown in the inset (a) of Fig. 5, where from bottom to top the data with fitting curves are given in the increasing order of U . Consequently, the spin-gap transition line $\Delta_{\sigma}(U)$ (circles with a fitting curve) is given in Fig. 5, where the reduced alternating potential parameter $\delta = \Delta / (\Delta + 2)$ is used as the y -axis. On the other hand, for the extrapolation of $\Delta_{\rho}(U, L)$, we assume the following formula:³⁶ $\Delta_{\rho}(U, L) = \Delta_{\rho}(U) + aL^{-3}$, and extrapolate the data of $L = 10-18$ as shown in the inset (b) of Fig. 5. Consequently, Fig. 5 shows that the critical line in the charge part (squares with a fitting curve) does not coincide with the spin-gap transition line, i.e., $\Delta_{\sigma}(U) < \Delta_{\rho}(U)$, and that the 2D parameter space $\{(u, \delta) \mid 0 \leq u, \delta \leq 1\}$ is separated into the MI, BI, and SDI phases with SDW, CDW and BCDW, respectively. Since the Hubbard gap provides a principal energy scale, and a shape of the boundary is roughly determined so that the magnitude of the band gap becomes comparable to the scale, the U dependence of the boundaries is expected to be weak in the small- U region,^{8,10} which is in agreement with our observation. On the other hand, in order to clarify the behaviors in the large- U region, we plot a magnification of the phase diagram around the $2\Delta = U$ line in Fig. 6. This shows that in the limit of $U \rightarrow \infty$ the boundaries do not merge to the line: More precisely, for $U = 96$ we obtain $\Delta_{\rho} - U/2 \simeq -0.65$ and $\Delta_{\sigma} - U/2 \simeq -0.97$, respectively. In the reference 16, adding to the spin part ($2\Delta_{\sigma} - U \simeq -1.91$ for $U, V \gg 1$), they also reported $2\Delta_{\rho} - U \simeq -1.33$, which is close to our estimation. Consequently, we confirm that the intermediate SDI phase may survive in the large- U limit, which is one of the nontrivial behaviors and is contrasted to the naive argument.

IV. DISCUSSION AND SUMMARY

For the understanding of the phase diagram in the large- U limit, let us see the perturbative treatment of Hamiltonian (1) under the condition of $U - 2\Delta \gg 1$. $\Delta_{\sigma}(U)$ may be related to the spin-gap transition point in the $S = \frac{1}{2}$ J_1 - J_2 model.^{10,20} Therefore using its numerical value²² and perturbative expressions on J_1 and J_2 ,⁶ we can approximately estimate $\Delta_{\sigma}(U)$ as a solution of the equation $J_2/J_1 \simeq X/(1 - 4X) \simeq 0.2411$, where $X = (1 + 4x^2 - x^4)/U^2(1 - x^2)^2$ and $x = 2\Delta/U$. Then, we find a solution $[\Delta'_{\sigma}(U)]$ to give a value $\Delta'_{\sigma}(U) - U/2 \simeq -1.427$ in the limit. While, due to the lack of effects from the higher order processes in the kinetic energy term, the approximate value deviates from the numerical estimation, this exhibits the following, i.e., the perturbative expan-

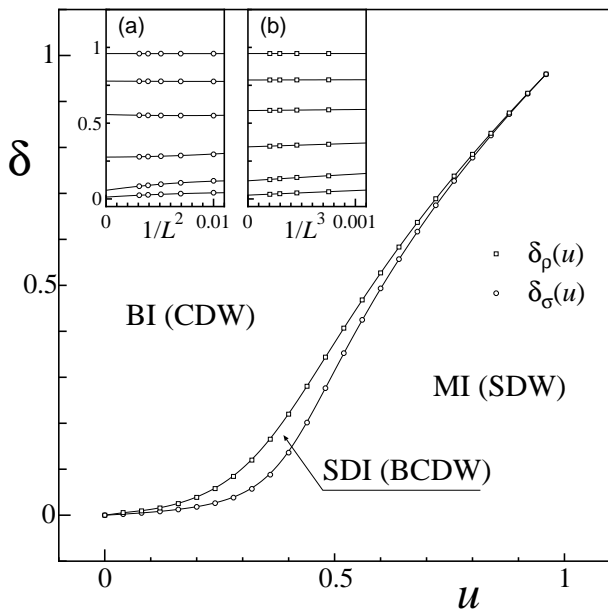


FIG. 5: The ground-state phase diagram of the 1D Hubbard model with the alternating potential. The circles (squares) with a fitting curve show the spin-gap (2D-Ising) transition line in the spin (charge) part. The stable regions of the MI, SDI and BI phases are given in the 2D parameter space (u, δ) [$u = U/(U + 4)$ and $\delta = \Delta/(\Delta + 2)$]. Insets (a) and (b) show the extrapolations of the L -dependent transition points in the spin and the charge parts, respectively.

sion becomes singular on the $2\Delta = U$ line so that the phase boundary deviates from the line. This singularity also exists in the perturbative calculations of the SDW and CDW state energies (E_{SDW} and E_{CDW}). And then the direct transition line between these phases cannot be determined from the equation $E_{\text{SDW}} = E_{\text{CDW}}$, which is highly contrasted to the case of the extended Hubbard model (EHM) including the nearest-neighbor Coulomb interaction $\sum_j V n_j n_{j+1}$.³⁷ Since the spin-charge coupling term with the dimerized spin part generates one of the relevant forces, $\Delta_\rho(U)$ should be affected by that of the spin part. Besides the present model, it is known that EHM possesses the coupling term $V \cos \sqrt{8}\phi_\rho \cos \sqrt{8}\phi_\sigma$ in its bosonized form,⁵ and that the BCDW state with the locking points $\langle \sqrt{8}\phi_{\rho,\sigma} \rangle = 0$ is stabilized around the $2V = U$ line in the weak- and intermediate-coupling region.²⁷ The corrections to g_ν from higher energy states stabilize it,³⁸ but the coupling term forces the boundaries to merge into the single first-order phase transition line between the SDW and CDW states in the strong-coupling region because it raises the BCDW state energy. However, in the present BCDW state, the locking point ϕ_0 in TABLE I may take a value so as not to bring about a large energy cost due to the coupling term Eq. (3). Therefore, the existence of the SDI phase is not prohibited even in the strong-coupling limit in contrast to the EHM case. Of course, these arguments are qualitative

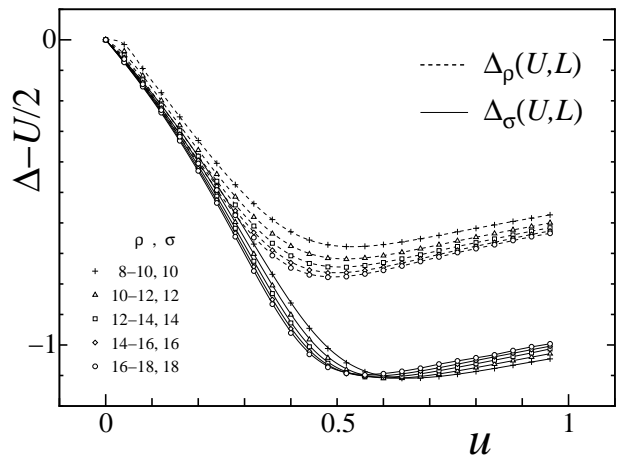


FIG. 6: The deviations of boundaries from the $2\Delta = U$ line, $\Delta_\nu(U, L) - U/2$. We use $u = U/(U + 4)$ as the x -axis. The correspondence between marks and system sizes is given in the figure. Marks with solid (dotted) curves exhibit the deviations in the spin (charge) part.

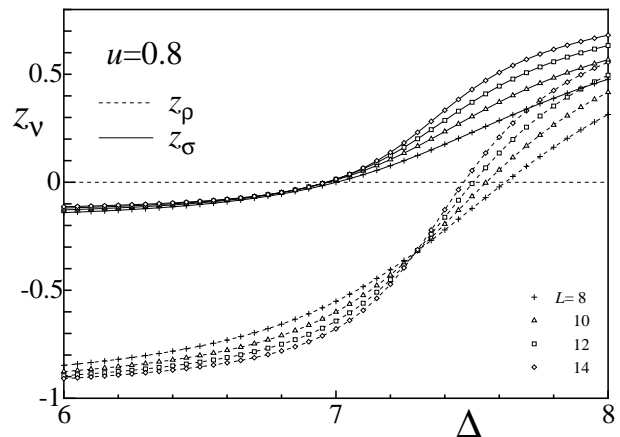


FIG. 7: Behavior of the ground-state expectation value of the twist operator z_ν ($\nu = \rho, \sigma$) near the $2\Delta = U$ line. The correspondence between marks and system sizes are given in the figure.

and intuitive ones, so an effective theory in this limit is required for the precise descriptions on the limiting behaviors.

Finally, we comment on the Berry phase method.^{9,13,14,15,16} The Berry phases for the charge and the spin parts γ_ν are related to the ground-state expectation values of the twist operators as $\gamma_\nu = \text{Im} \log z_\nu$ where

$$z_\rho = \langle U_\uparrow U_\downarrow \rangle, \quad z_\sigma = \langle U_\uparrow U_\downarrow^{-1} \rangle, \quad (14)$$

and $U_s = \exp[(2\pi i/L) \sum_{j=1}^L j n_{j,s}]$.¹³ Since z_ν is real at the half-filling with zero-magnetic field, γ_ν ($=0$ or π) indicates the sign of z_ν . On one hand, z_ν can be related

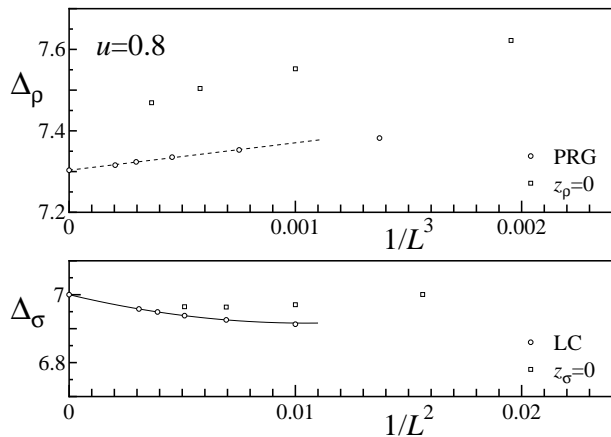


FIG. 8: Comparisons of the system-size dependences of the transition points obtained by the LC and PRG methods versus by the condition $z_\nu = 0$. The fitting curves show the extrapolations of data to the thermodynamic limit.

to the bosonic field as $z_{\rho,\sigma} \propto \mp \langle \cos \sqrt{8}\phi_{\rho,\sigma} \rangle$, so that it includes the information of the locking points given in TABLE I.¹⁵ In Fig. 7 we show behaviors of z_ν near the $2\Delta = U$ line for $U = 16$ and find that with the increase of Δ both of these increase and change their sign. As shown in the lower panel of Fig. 8, the condition $z_\sigma = 0$ gives a close value to the result of the LC method, so it may provide a proper estimation of the spin-gap transition point Δ_σ .^{15,16} On the other hand, the zero point of z_ρ exhibits a deviation from the PRG result (see the upper panel of Fig. 8). Since ϕ_0 continuously varies with Δ , z_ρ can take a finite value on the 2D-Ising transition point in the thermodynamic limit, which is highly contrasted to z_σ on the spin-gap transition point. In fact, the size-dependent zero points are seemingly extrapolated to a value different from our PRG estimation, so that the condition $z_\rho = 0$ does not specify the transition point. On the other hand, we also find in Fig. 7 that there is a point $\Delta \simeq 7.3$ at which z_ρ is almost independent of L . This crossing point is expected to be a good estimator for the 2D-Ising transition point in the charge part Δ_ρ because this is quite close to the PRG result even for small L . However, a theoretical explanation of this possibility is still open.

To summarize, we have investigated the ground-state phase diagram of the one-dimensional half-filled Hubbard model with the alternating potential, especially in order to verify the new scenario given by Fabrizio, Gogolin,

and Nersesyan, we have numerically treated the phase transitions observed in the spin and charge parts: We calculated the spin-gap transition points Δ_σ in the spin part by the level-crossing method (see also the argument for the spin-gap transition in Ref. 16) and the two-dimensional Ising transition points Δ_ρ in the charge part by the phenomenological renormalization-group method. We confirmed that, adding to the Mott and band insulators, the “spontaneously dimerized insulator” accompanied by the long-range-ordered $2k_F$ bond charge-density wave is stabilized as the intermediate phase for all $U > 0$. Then we checked the SU(2)-symmetric Gaussian (2D-Ising) criticality of the spin (charge) part by treating the low-lying excitation levels in the finite-size systems, and simultaneously we performed the finite-size-scaling analysis of the charge-excitation gap to clarify the critical phenomena around Δ_ρ . The comparison with the relating work was performed to check the reliability of our numerical results and to exhibit the efficiency of our approach.

After submission of this article, we became aware of the work investigating the ground-state phase diagram and the universality of the transition in the charge part by the use of finite-size-scaling analysis of the DMRG calculation data.³⁹ They have found two transition points and succeeded to obtain $\nu = 1$ in agreement with our conclusion, while the estimated exponent for the susceptibility of the BCDW order parameter shows a deviation from the expected value. In this paper we have treated the elementary excitations in the TLL system specified by utilizing the discrete symmetries of the lattice Hamiltonian, while they have measured the BCDW order parameter, (i.e., a composite excitation of the spin and charge degrees of freedom) with the larger energy scale.

ACKNOWLEDGMENTS

One of the author (H.O.) is grateful to Y. Okabe for helpful discussions. M.N. thanks J. Voit for the collaboration in the early stage of the present work. M.N. is partly supported by the Ministry of Education, Culture, Sports, Science and Technology of Japan through Grants-in-Aid No. 14740241. Main computations were performed using the facilities of Tokyo Metropolitan University, Yukawa Institute for Theoretical Physics, and the Supercomputer Center, Institute for Solid State Physics, University of Tokyo.

¹ J. Kanamori, Prog. Theor. Phys. **30**, 275 (1963); J. Hubbard, Proc. R. Soc. London A **276**, 238 (1963); M.C. Gutzwiller, Phys. Rev. Lett. **10**, 59 (1963).

² S. Tomonaga, Prog. Theor. Phys. **5**, 544 (1950); J.M. Luttinger, J. Math. Phys. **4**, 1154 (1963).

³ F.D.M. Haldane, J. Phys. C **14**, 2585 (1981).

⁴ H. Frahm and V.E. Korepin, Phys. Rev. B **52**, 10 553 (1990); N. Kawakami and S.-K. Yang, Phys. Lett. A **148**, 359 (1990).

⁵ For example, J. Voit, Phys. Rev. B **45**, 4027 (1992).

- ⁶ N. Nagaosa and J. Takimoto, J. Phys. Soc. Jpn. **55**, 2735 (1986). See also N. Nagaosa and J. Takimoto, J. Phys. Soc. Jpn. **55**, 2745 (1986); N. Nagaosa, *ibid.* **55**, 2754 (1986); *ibid.* **55**, 3488 (1986).
- ⁷ T. Egami, S. Ishihara, and M. Tachiki, Science **261**, 1307 (1993); S. Ishihara, T. Egami, and M. Tachiki, Phys. Rev. B **49**, 8944 (1994); *ibid.* **49**, 16 123 (1994).
- ⁸ M. Tsuchiizu and Y. Suzumura, J. Phys. Soc. Jpn. **68**, 3966 (1999).
- ⁹ R. Resta and S. Sorella, Phys. Rev. Lett. **74**, 4738 (1995); *ibid.* **82**, 370 (1999).
- ¹⁰ M. Fabrizio, A.O. Gogolin, and A.A. Nersesyan, Phys. Rev. Lett. **83**, 2014 (1999);
- ¹¹ M. Fabrizio, A.O. Gogolin, and A.A. Nersesyan, Nucl. Phys. B **580**, 647 (2000).
- ¹² T. Wilkens and R.M. Martin, Phys. Rev. B **63**, 235108 (2001).
- ¹³ R. Resta, Phys. Rev. Lett. **80**, 1800 (1998).
- ¹⁴ A. Aligia and G. Ortiz, Phys. Rev. Lett. **82**, 2560 (1999).
- ¹⁵ M. Nakamura and J. Voit, Phys. Rev. B **65**, 153110 (2002).
- ¹⁶ M.E. Torio, A.A. Aligia, and H.A. Ceccatto, Phys. Rev. B **64**, 121105 (2001).
- ¹⁷ Y. Takada and M. Kido, J. Phys. Soc. Jpn. **70**, 21 (2001).
- ¹⁸ J. Lou *et al.*, Phys. Rev. B **68**, 045110 (2003).
- ¹⁹ Y.Z. Zhang, C.Q. Wu, and H.Q. Lin, Phys. Rev. B **67**, 205109 (2003).
- ²⁰ A.P. Kampf *et al.*, J. Phys. C **15**, 5895 (2003).
- ²¹ H.H. Roomany and H.W. Wyld, Phys. Rev. D **21**, 3341 (1980).
- ²² K. Okamoto and K. Nomura, Phys. Lett. A **169**, 433 (1992).
- ²³ K. Nomura and K. Okamoto, J. Phys. A **27**, 5773 (1994).
- ²⁴ For example, A. Kitazawa, K. Nomura, and K. Okamoto, Phys. Rev. Lett. **76**, 4038 (1996); A. Kitazawa and K. Nomura, J. Phys. Soc. Jpn. **66**, 3944 (1997).
- ²⁵ M. Nakamura, Physica B **329-333**, 1000 (2003); M. Nakamura, T. Yamamoto and K. Ide, J. Phys. Soc. Jpn. **72**, 1022 (2003); K. Okamoto, Phys. Rev. B **67**, 212408 (2003).
- ²⁶ M. Nakamura, K. Nomura, and A. Kitazawa, Phys. Rev. Lett. **79**, 3214 (1997).
- ²⁷ M. Nakamura, J. Phys. Soc. Jpn. **68**, 3123 (1999); Phys. Rev. B **61**, 16377 (2000).
- ²⁸ H. Otsuka, Phys. Rev. B **66**, 172411 (2002).
- ²⁹ For a recent review, see A.O. Gogolin, A.A. Nersesyan, and A.M. Tsvelik, *Bosonization and Strongly Correlated Systems* (Cambridge University Press, Cambridge, 1998).
- ³⁰ A.B. Zamolodchikov, Zh. Eksp. Teor. Fiz. **43**, 565 (1986) [JETP Lett. **43**, 730 (1986)].
- ³¹ G. Delfino and G. Mussardo, Nucl. Phys. B **516**, 675 (1998).
- ³² J. Cardy, J. Phys. A **17**, L385 (1984).
- ³³ Z. Bajnok, L. Palla, O. Takács, and F. Wágner, Nucl. Phys. B **601**, 503 (2001).
- ³⁴ H.W. Blöte, J. Cardy, and M.P. Nightingale, Phys. Rev. Lett. **56**, 742 (1986); I. Affleck, *ibid.* **56**, 746 (1986).
- ³⁵ For example, M.N. Barber, in *Phase Transitions and Critical Phenomena*, edited by C. Domb and M.S. Green (Academic Press, London, 1983), Vol. 8.
- ³⁶ C. Itzykson and J.-M. Drouffe, *Statistical Field Theory*, (Cambridge University Press, New York, 1989). Vol. 1; T. Sakai and M. Takahashi, J. Phys. Soc. Jpn. **59**, 2688 (1990).
- ³⁷ P.G.J. van Dongen, Phys. Rev. B **49**, 7904 (1994).
- ³⁸ M. Tsuchiizu and A. Furusaki, Phys. Rev. Lett. **88**, 056402 (2002).
- ³⁹ S.R. Manmana *et al.*, cond-mat/0307741(unpublished).